LAWRENCE
LIVERMORE
NATIONAL
LABORATORY

UCRL-JRNL-219331

Laser light Backscatter from Intermediate and High Z plasmas

R. L. Berger, C. Constantin, L. Divol, N. Meezan, D. H. Froula, S. H. Glenzer, C. Niemann, L. J. Suter

February 27, 2006

Physics of Plasmas

Laser light Backscatter from Intermediate and High Z plasmas

R. L. Berger, C. Constantin, L. Divol, N. Meezan, D.
H. Froula, S. H. Glenzer, C. Niemann, and L. J. Suter*
University of California, Lawrence Livermore National Laboratory,
P. O. Box 808, Livermore, CA 94551

(Dated: 9 February 2006)

Abstract

In experiments at the Omega Laser Facility, stimulated Brillouin backscatter (SBS) from gasbags filled with Krypton and Xenon gases was unexpectedly 10 times lower than from CO_2-filled gasbags with similar electron densities. The SBS backscatter was a 1-5 % for both 527nm and 351nm interaction beams at an intensity of $\sim 10^{15}$W/cm^2. The SRS backscatter was less than 1%. The 351nm interaction beam is below the threshold for filamentation and all the SBS occurs in the density plateau between the blast waves. Inverse bremsstrahlung absorption of the incident and SBS light account for the lower reflectivity from Kr than from CO_2. The 527nm interaction beam filaments in the blowoff plasma before the beam propagates through the blast wave where it is strongly absorbed. Thus, most of the 527nm SBS occurs in the flowing plasma outside the blast waves. Nonlinear processes that limit the acoustic wave amplitudes to 1% of electron density model the SBS reflectivity well in both CO_2 and Krypton plasmas .

*Electronic address: berger5@llnl.gov

I. INTRODUCTION

Stimulated Brillouin scattering (SBS) of laser light from ICF plasmas constrains the design of ignition targets for the National Ignition Facility.[1] Designs under consideration involve the propagation of light through low charge state (Z) plasma mixtures such as HeH and CH, intermediate Z plasma mixtures such as SiO_2, and high Z plasma such as gold. The gain of SBS is higher and threshold of SBS is lower as the ion acoustic wave damping decreases. The dispersion properties of acoustic waves in hot, low density plasmas are very similar for intermediate and high-Z plasma because $ZT_e/T_i \gg 1$ and ion Landau damping is negligible. Experiments with hohlraum targets at the former NOVA Laser Facility[2] measured SBS that was consistent with scattering from gold plasma that was ablated from the hohlraum wall.[3] In order to better understand the nonlinear SBS interaction for weakly damped ion acoustic waves, CO_2 gasbag plasmas were used in experiments at NOVA [4] as a surrogate for gold in studying SBS in long scale length plasma because of the difficulties of creating long scale length gold plasmas. However, collisional processes are much stronger in gold than CO_2. Thus Krypton ($Z \sim 30$) or Xenon ($Z \sim 40$) rather than a CO_2 plasma should provide a much better approximation to a gold plasma because of their similar collisional damping and light absorption processes.

Experiments at the Omega laser facility[5] have reported [6] that the stimulated Brillouin backscatter (SBS) from Krypton (Kr) and Xenon filled bags is 1-5% for incident laser intensity of $\sim 8 \times 10^{14}\mathrm{W/cm^2}$ for both 351nm and 527nm laser wavelengths. Stimulated Raman backscatter was even smaller ($< 1\%$). This small SBS was somewhat unexpected given the large SBS ($\gtrsim 30\%$) reported from gasbags filled with CO_2 to equivalent fully ionized electron densities[4] and the fact that ion acoustic waves in CO_2 and Krypton plasmas have similar dispersion properties. The ion Landau damping is negligible and the electron Landau damping ν_a is small, about $0.01\omega_a$ where $\omega_a \sim k\sqrt{ZT_e/m_i}$. In Krypton plasmas, the ion-ion mean free path, $\lambda_{ii} \propto n_i^{-1}Z^{-4}$, is small enough that $k\lambda_{ii} \lesssim 1$ so viscous damping must be included. However, that damping rate is only about as large as electron Landau damping so ion acoustic waves remain weakly damped. This large difference in SBS reflectivity of CO_2 and Krypton plasmas cannot be explained with linear damping of the acoustic waves.

Because of the high charge state of Krypton, $Z_{Kr} \sim 30$ and Xenon, $Z_{Xe} \sim 40$, inverse bremsstrahlung absorption is stronger and classical thermal conduction is weaker than in

CO_2 ($Z_{CO_2} = 7.3$) plasma with the result that electron temperatures in Krypton and Xenon are about 50% higher than those in CO_2 for the same electron density. The SBS growth rate and gain rate which are inversely proportional to T_e might cause lower SBS reflectivity from higher Z plasmas if the gain is in the range (~ 25) where a change of less than two can have a dramatic effect.

For 527 nm light, a quantitative analysis of the SBS gain from Krypton plasmas shows that most of the SBS occurs in the expanding plasma (blowoff) because of the strong absorption of the incident and reflected light by the blast wave (the higher-than-average density plasma at the edges of the bag, *e.g.* see Fig. 5) whereas, for the 351 nm light, the analysis of the gain shows that most of the SBS occurs in the plateau. The 527 nm SBS light amplification is limited by the velocity gradient of the expanding plasma. The 351 nm light backscatter is determined by a combination of (weak) plasma gradients, temporal incoherence acquired in propagating through the blast waves, and absorption of the incident and reflected light. Because the power of the typical speckle is above the ponderomotive self-focusing threshold for 527 nm light in the plasma blowoff, filamentation and beam spray plays an important role in SBS. In this region, the strong gradients and weak ion acoustic wave damping limit the growth to less than a speckle length. Filamentation is below threshold for 351 nm light.

Quantitative modeling of the backscatter from all targets also demands that the ion wave amplitude be nonlinearly limited to about 1% of the background density for both 527 and 351 nm incident light and for both Kr and CO_2 gasfills. Previous experiments [3, 4] and subsequent modeling [7] have also shown the need for nonlinear processes that limit the ion acoustic wave amplitude. Here, we show that the same nonlinear modeling applies successfully to both CO_2 with 25-30% SBS and Krypton plasmas with 1-5% SBS provided the laser propagation through the entire plasma, including the blast waves, is included. Moreover, by including additional physical processes, the ion wave amplitudes that are consistent with the level of SBS are nearly an order of magnitude larger than used in previous modeling and are more consistent with levels found in kinetic simulations.[8, 9].

In Section II, the experiment is described and the stimulated Brillouin and Raman backscatter results are presented. Section III discusses the radiation-hydrodynamic simulation of the plasma properties and establishes their validity by comparison with measurements. The relevant linear theory of ion acoustic waves and the thresholds and gains for

stimulated Brillouin scattering for the plasma conditions established in Sec. III are presented in Sec. IV. In Sec. V, we present 2D simulations of the propagation and SBS of the 351 nm and 527 nm laser light through Krypton and CO_2 gasbags and show the importance of inverse bremsstrahlung, plasma inhomogeneity, and plasma-induced laser incoherence in determining the reflectivity. Without the absorption of the incident and reflected light by the blast waves, the Kr SBS would be similar to the CO_2 SBS. However, the SBS spectral shifts from the 2D simulations of 527 nm light propagation do not agree with the data for 527nm incident light. In Sec. VI, we present 3D simulations of the light propagation through the flowing plasma and show the importance of hotspots, filamentation, and nonlinear limits on plasma waves in reproducing the measured 527 nm SBS spectrum. We conclude in Sec. VII

II. EXPERIMENT DESCRIPTION

The experiments were performed at the OMEGA laser facility. A total of 19.5 kJ of 351nm laser light in 1ns square "heater" pulses irradiate the target. Most of the SBS and SRS data were obtained with the focus of all the heater beams 3.5 mm beyond target center as shown in Fig. 1. The heater beam overlap region is about 800μm. In addition two nonoverlapping "interaction" beams smoothed with a phase plate and focused to the center of the gasbag with an f/6.7 lens to an intensity of 8×10^{14}W/cm^2 in a 250μm spot irradiate the target. One interaction beam has wavelength 351 nm and the other 527 nm. Each interaction beam pulse is delayed by 500ps after the start of the heater pulse.

The plasma is formed by ionizing a gas contained within 0.35μm thick polyimid membranes supported by a 0.7 mm thick aluminum washer. The bags are filled with Krypton or CO_2 to pressures between 0.48 atm and 1.47 atm which result in electron densities for Krypton fills between $.04N_c^{351}$ and $0.11N_c^{351}$. The experiment was previously described and analyzed for the radiation conversion efficiency.[6] Here, we present the light scattering results and describe the backscattered light diagnostics.

The light backscattered from the interaction beams was collected by the full aperture backscatter station (FABS). When these data were taken, the SBS included only the light reflected into the focusing optics of the incident light. In the simulations (described in Sec V), more than 80% of the backscatter of the 351nm light is reflected into the incident light

cone. For 527 nm light, most of the simulated backscatter is outside the incident light cone.

The example of a streaked spectrum of SBS in Fig. 2 is typical of the 351 nm SBS in that the peak scatter occurs just as the heater beam power is turned off. After that time SBS decreases as the plateau density region shrinks. The rate of increase of SBS shown in the lineout in Fig. 2 is affected by the ramp up of the interaction beam and the response time of the spectrometer, both of which are ~ 200 ps.

In a stationary plasma, the peak SBS occurs for light shifted in frequency by the acoustic wave frequency. The backscattered light wavelength is then

$$\Delta\lambda \simeq \lambda_0 \frac{2C_s}{c} = \frac{21.7}{h}\sqrt{\frac{ZT_e}{A}}\mathring{A} \tag{1}$$

where $h = 2$ for 527 nm light and $h = 3$ for 351 nm light, Z is the charge state, and A is the atomic number. The spectrum in Fig. 2 shows a narrow line shifted with respect to the incident light by 6.5 $\mathring{A}$, close to the value expected from Eq. (1). This data, typical of the SBS of a 351nm interaction beam from Krypton targets, consists of a narrow line about 1 Å in width whose shift from the incident light wavelength increases monotonically with fill density from ~ 5 $\mathring{A}$ to 8 $\mathring{A}$. The shift from CO_2 targets for backscatter of 351 nm light is also a narrow line consistent with backscatter from the plateau. The 527 nm spectra are completely different in that the spectra are not narrow with peaks that are increasingly less redshifted as the fill density increases and that are best explained if the SBS occurs in the expanding plasma exterior to the blast wave. SBS 527 nm spectra from the lower density Krypton fills and the CO_2 fills has two components that are likely from the plateau (the fainter signal and larger redshift) and the expanding plasma (the brighter signal).

The electron temperature measurements were performed with two different Thomson probe beam configurations by means of collective Thomson scattering ($\alpha = 1/\mathrm{k}\lambda_\mathrm{D} > 1$). Initial measurements were accomplished with a 527 nm laser probe beam that is restricted to the edge of the plasma because of strong absorption and refraction of the probe. The heater beams in this case were focused 3.5 mm beyond the target center as shown in Fig. 1. The installation of a 4ω (266 nm) Thomson scattering diagnostic (TSD) allowed new measurements of the plasma temperature in the center of the gasbags. The beam configuration in this set of experiments, also shown in Fig. 1 with a schematic of the Thomson scattering setup,[10] was somewhat different (the SBS spectral shifts listed in Table I and the hydrodynamic simulations indicate that the electron temperature is weakly dependent on the

TABLE I: The measured SBS spectral shift

		$\lambda_0 = 351$ nm		$\lambda_0 = 527$ nm		
N_e/N_c^{351}	Gas	$\Delta\lambda_0(\AA)$	width (Å)	$\Delta\lambda_0(\AA)$	width (Å)	Omega Shot number
.05	CO_2	8	1.5	3	6	27692
.065	CO_2	8	1	5.6	3	27691
.03	Kr	5	1	3	7	29677[a]
.05	Kr	5.5	2	1.4	8	29676
.06	Kr	6.5	1	-	-	32053[b]
.07	Kr	7	2	1.4	8	29674
.09	Kr	7.5	1	-1	10	29678

[a]The 527 nm interaction beam energy was about 1/3 of the other shots.

[b]There was no 527 interaction beam because this shot had Thomson scattering which uses the same beamline.

focusing differences). This TSD had a time resolution of 100 ps and a spectral resolution of 0.5 Å. The scattering volume was $200 \times 200 \times 200\mu$m for both probe wavelengths.

In Fig. 3, the TS data for the $6\%N_c^{351}$ Krypton fill from a scattering volume near target center is shown from the same shot as the SBS data shown in Fig. 2. The peak-to-peak separation (ignoring the bright central peak of stray light) is about 0.65 nm. The temperature deduced from the fitting the TS spectrum with the shape determined theoretically is 3-3.5 keV in the period 0.5-0.8 ns into the heater pulse.[11] At 1.3 ns, 0.3 ns after the heater beams turn off, the electron temperature deduced is 1.8-2.0 keV near target center. The charge state used in determining the electron temperature from the Thomson spectra was Z = 26 as calculated by the radiation-hydrodynamic modeling (see Sec. III). The temperatures are accurate to ±20%. These measurements are in very good agreement with the modeling presented in Sec. III.

The time-integrated SBS reflectivity from the Krypton gas filled targets is shown in Fig. 4 for both 351 nm and 527 nm interaction beams. The 351 nm reflectivity decreases montonicallywith density while the 527 nm reflectivity increases with density except for the highest density fill. From the data in Table I, we know that the 527 nm SBS is primarily from the expanding plasma, not the plateau. If only the plateau SBS were plotted, the 527

nm reflectivity would be much smaller and would decrease with density.

III. SIMULATED PLASMA CONDITIONS

Radiation-hydrodynamics simulations of the gasbags were performed with HYDRA to assist in the analysis of the experiments. HYDRA is a 2D/3D multi-physics code based originally on a hydrodynamics package by R. Tipton and developed by M. Marinak for inertial confinement fusion simulations [12]. HYDRA's laser ray-tracing package includes inverse bremsstrahlung absorption, bulk refraction, and turning-point energy deposition, but does not simulate speckle-scale laser-plasma physics. The gasbags were simulated in 2D as oblate spheroids, with the axis of rotation perpendicular to the aluminum washer. The major axis, corresponding to the inner diameter of the washer, was 2.75 mm, while the minor axis was 2.4 mm. A 351 nm or 527 nm interaction beam was sent along the axis of rotation. The interaction beam has little effect on the bulk plasma properites. The 39 heater beams were divided into 6 or 10 beam cones for the simulations to mimic the actual pointing of each experiment, with 200 laser rays per beam.

The aluminum washer was included in the simulations. Electron thermal conduction from the heated gas plasma to the solid washer plays an important role in determining the electron temperature in the gas. A gradient driven (local) model for electron thermal conduction was used for these simulations. For the local model, the maximum heat flux allowed across a given surface is some fraction f (the flux limiter) of the "free-streaming" heat flux,

$$q = \min(-\kappa \nabla T_e, f \times q_{fs}), \tag{2}$$

where

$$q_{fs} = (n_e k_B T_e)\, v_{te}. \tag{3}$$

Here, n_e is the electron density, T_e is the electron temperature, k_B is Boltzmann's constant and $v_{te} = \sqrt{k_B T_e / m_e}$ is the electron thermal velocity. These simulations used a weak flux-limiter of 1. The quotidian equation of state (QEOS) [13] with separate electron and ion temperatures was used for all materials. The non-local-thermodynamic -equilibrium (non-LTE) atomic physics model XSN [14] was used to generate opacities and calculate the ionization states of the materials. Previous HYDRA simulations of gasbag targets showed good agreement with experimental diagnostics [15].

The rapid heating and explosion of the membranes compresses the gas on the inside to form a "blast wave" about 0.2mm thick. The peak density of the blast wave is about twice the fill gas electron density. The Krypton plasma formed has a rather uniform electron density plateau in the region between the blast waves.

Representative Krypton plasma conditions 700ps after the 351nm wavelength heating laser beams have illuminated the gasbags are shown in Fig. 5 for the $.04N_c^{351}$ gasfill. The electron temperature is highest at the center of the plasma and coolest at the edge where the electron pressure is driving a hydrodynamic expansion. At the plasma edge, there are significant gradients in the plasma flow velocity and density that act to limit the amplification of SBS and SRS respectively.

The CO_2 plasma conditions for the $.04N_c^{351}$ gasfill at 700ps are also shown in Fig. 5. Here the electron temperature is about 2.6keV at the center, varies by less than 200eV between the blast waves. The ion temperature in the plateau region of the CO_2 plasma is lower than in Krypton because the temperature equilibration rate is slower at lower Z for a given electron temperature. Thus, the electrons must be heated more for a higher Z plasma before the ion temperature decouples from the electron temperature. However, it is interesting that the flow velocity profile shown in Fig. 5 is the same for CO_2 and Krypton plasmas of the same fill density. A simple explanation for the similar flow velocity profiles is that the flow velocity scales with the sound speed $C_s = \sqrt{Z(T_e + 5T_i/3)/m_i}$ which is very nearly the same although Z, T_e, and m_i for the two materials differ.

In the plateau, the plasma electron temperature is determined by a balance of the amount of energy absorbed from the 39 heater laser beams against the heat capacity of the gas, hydrodynamic expansion losses, radiation loss,[6] and the loss to the washers that initially support the membranes . For the intermediate fill densities ($.05 - .08N_c^{351}$), the electron temperatures have nearly the same spatial and temporal dependence. The maximum temperature is at the center of these bags with a value that increases from 3.8keV at 500ps to 4.2keV at 900ps in good agreement with the Thomson scattering measurements reported in Sec. II. After the 39 heating beams turn off at 1ns, the temperatures decrease from hydrodynamic and radiation losses to less than 2.8keV by 1.3ns. The higher density fill takes longer to heat up and reaches its maximum temperature of 3.9keV at 900ps. Because the lowest density fill absorbs about 50% of the heater beam energy after 500ps whereas the higher density fill absorbs more than 70%, its peak temperature is about 500eV lower.

The charge state of Krypton for all the gas fills is spatially uniform with value $Z_{Kr} \sim 30$. The charge state calculated in the simulations is nearly the same as used in deducing an electron temperature from the Thomson scattering data. The measured and simulated temperature agree well while the heaters are on. The simulation has a higher electron temperature at 1.3 ns by 0.5 keV than deduced from Thomson scattering.

The blast waves move into the stationary plasma at the sound speed and form a shock in which the ion temperature is elevated to $5 - 20$keV, far above the electron temperature. In the blast wave, the density is higher and the ion temperature is lower for the higher density fills.[16] The ion temperature in the plateau region is less than 1keV. Although the electron density is initially uniform, the gradient in the electron pressure pushes plasma out from the center of the bag and lowers the density at the center. As the blast wave moves inward, the length of the plateau region shrinks with time from nearly 2mm to $\sim$ 1mm by 1.1ns.

In the region exterior to the blast waves, the plasma expands similarly to a laser-heated disk or thin foil where the density drops exponentially and the magnitude of the velocity increases linearly.[17] The velocity profiles for all the Krypton fills are quantitatively the same. However, the density N_e, electron temperature N_e, and N_e/T_e are higher at a given flow velocity for the higher density fills. This scaling is important to understanding the SBS from 527 nm incident light.

IV. STIMULATED BRILLOUIN SCATTERING: LINEAR REPONSE

Absorption of the incident light is a dominant factor for these high-Z plasmas because the inverse bremsstrahlung intensity absorption rate,

$$\kappa_{ib} \;=\; \frac{N_e}{N_c}\frac{\nu_{ei}}{|\mathrm{v_g}|}, \tag{4}$$

is proportional to the charge state of the ion, Z, through the rate's dependence on the electron-ion collision frequency,

$$\nu_{ei} \;=\; 4\sqrt{(2\pi)}N_e Z e^4 \ln\Lambda / \left(3m_e^2 V_e^3\right). \tag{5}$$

In Eq. (4), the light wave group velocity in the plasma is $\mathrm{v_g} = \sigma \mathrm{c}\sqrt{1 - \mathrm{N_e/N_c}}$ where $\sigma = \pm 1$ for the incident and reflected light respectively. Here, m_e is the electron mass, e is the electron charge, V_e is the electron thermal velocity, c is the speed of light in vacuum,

N_e is the electron density, N_c is the critical density for light of frequency ω_0, and $\ln\Lambda$ is the Coulomb logarithm appropriate for absorption. The charge state for Krypton ($Z \sim 30$) is about 4× larger than that for CO_2 ($\overline{Z} = 7.3$) which has the effect of reducing the absorption length and increasing the electron temperature in Krypton plasma with respect to CO_2 plasma.

The 527nm and 351nm laser intensity spatial profiles for the interaction beams in the $4\%N_c^{351}$ Krypton and $4\%N_c^{351}CO_2$ gasfills are shown in Fig. 6. For the Krypton-filled bags, the laser light is strongly absorbed in the high-density blast waves at the edge of the density plateau. The least reduction is for the 351nm laser propagating into the $4\%N_c^{351}$ bag; the strongest reduction is for the 527nm laser propagating into the $11\%N_c^{351}$ bag.[18] For the CO_2 filled bags, the blast waves absorb much less light and the 351 nm laser intensity is highest in the plateau region.

In low-Z gas-filled bags, the stimulated scattering occurs mostly in the plateau region between the blast waves. In these high-Z plasmas, a boost in the amplification occurs in the plasma expansion where the flow velocity passes through zero because the laser intensity is higher there than in the plateau because of absorption as the laser light passes through the blast wave. This absorption by the blast wave is particularly important for the 527nm laser light because of the factor N_e/N_c in the spatial absorption rate, κ_{ib}. In Fig. 7, the calculated transmission fraction of light through the blast wave (without accounting for backscatter) is shown for 351nm and 527nm laser light. For the 527nm light about 50% of the light penetrates the blast wave for the lowest density fills but only 10% at $0.11N_c^{351}$ fill density.

A. Linear Ion acoustic wave dispersion

As discussed previously, the linear ion Landau damping for intermediate to high Z plasmas when $T_i < T_e$ is negligible because there are very few ions at the phase velocity of the wave. Assuming the collisionless dispersion relation is appropriate for the moment, the only damping is electron Landau damping. Using the cold ion response, one can solve the dispersion relation to find the frequency, ω_a, and amplitude damping rate, ν_a,

$$\omega_a \;=\; k\sqrt{\frac{ZT_e/m_i}{1+k^2\lambda_{de}^2} + \gamma_i T_i/m_i}, \tag{6}$$

$$\nu_a/\omega_a \;=\; \frac{\frac{1}{2}\sqrt{\pi/2}\sqrt{Zm_e/m_i}}{(1+k^2\lambda_{de}^2)^{3/2}}. \tag{7}$$

In Eq. (6), the value of γ_i ($5/3 < \gamma_i < 3$) is unimportant because the ion temperature contribution to the frequency is negligible. In Eq. (7), the very small ion contribution to the Landau damping is neglected. If $k\lambda_{de} \ll 1$ and Z/A = 1/2 where $A \equiv \mathrm{m_i/m_p}$ and $\mathrm{m_{p,i}}$ is the mass of a proton, ion, then $\nu_a/\omega_a \cong .01$. For hot low density plasmas, $k\lambda_{de} \sim 1$ and the electron Landau damping is even smaller. For high Z plasma, Z/A < 1/2 which also reduces the linear Landau damping. Not accounted for in Eq. 7 are collisional effects which play a role when $k\lambda_{ii} \lesssim 1$. For a single species plasma, the damping from ion viscosity has been computed as a function of $\mathrm{ZT_e/T_i}$ and $k\lambda_{ii}$.[19, 20] For the Krypton gasfills in the plateau region, $k\lambda_{ii} \sim 0.1 - 0.5$ for which, coincidentally, the viscous damping has a broad maximum value (as a function of $k\lambda_{ii}$) of $\nu_a^{vis} = .03\mathrm{kv_i}$ where $v_i = \sqrt{T_i/m_i}$ is the ion thermal velocity. Thus, $\nu_a^{vis}/\omega_a = .03\sqrt{T_i/ZT_e}\sqrt{1+k^2\lambda_{de}^2} \sim .003$ which is small because $\mathrm{T_i} \ll \mathrm{ZT_e}$. However, it is about the same magnitude as the electron Landau damping for Krypton plasmas. For CO_2 parameters, $k\lambda_{ii} \sim 10$ and this viscous damping is an order of magnitude smaller, $(\nu_a^{vis}/\omega_a)_{\mathrm{CO_2}} \sim 10^{-4}$.

In the lowest density Krypton fill and for 351nm incident laser light, the wavelength of the SBS-driven acoustic wave, $\lambda = 2\pi/k \sim \lambda_0/2$, is comparable to the electron Debye length $\lambda_{de} = V_e/\omega_{pe} \sim \sqrt{T_e/N_e}$ and thus the acoustic wave frequency is dependent on $k\lambda_{de}$ in addition to $kC_s = k\sqrt{ZT_e/m_i}$. The variation in $k\lambda_{de}$ across the plasma places additional limits on the SBS amplification. In Fig. 8, the variation of the local acoustic wave frequency in space is shown for various approximations for the nominal $4\%N_c^{351}$ gasbag. There, one can see about a 20% effect on the acoustic wave frequency from $k\lambda_{de}$ for the 351nm wavelength laser wave that reduces the frequency shift from the nominal kC_s. The $k\lambda_{de}$ factor also is evident in the blast wave where the density changes rapidly; however, the Doppler shift from the flow velocity variation is larger.

B. Nonlinear Ion wave processes

The ion acoustic waves responsible for SBS backscatter are driven typically and in these experiments also to large enough amplitudes that nonlinear fluid and kinetic effects are important. Examples of fluid nonlinearities are ion wave decay[8, 21–25] and harmonic

generation.[24, 26] In the former, the large amplitude ion wave decays into two longer-wavelength, lower-frequency ion waves which drains away some of its power. In contrast, in harmonic generation shorter wavelength ion waves are generated as the wave steepens, a well-known phenomenon in hydrodynamics as well. Ions and electrons can be trapped if they travel near the phase velocity of the wave and thereby alter both the Landau damping and the natural frequency of oscillation. The trapping of ions has been studied extensively in kinetic simulations and the magnitude and sign of the frequency shift has been obtained in both one and two dimensional simulations.[8] Electron trapping also causes a frequency shift of a similar magnitude but opposite sign.[27, 28] Electrons are trapped and alter the linear response for very small wave amplitudes because the electron trapping velocity is much larger than the ion trapping velocity, $V_{tr} = \sqrt{e\phi_a/m_s}$, where s = e, i for electrons and ions respectively. The electron trapping velocity equals the phase velocity when $e\phi_a/T_e = \delta n_a/n = Zm_e/(2m_i)$ whereas, for ions, this occurs only when $\delta n_a/n \sim 1$.

For CO_2 and Krypton plasmas, since there are very few ions at the phase velocity, ion trapping has little effect. Because $k\lambda_{de}$ of the primary acoustic wave may be large (> 0.4), the harmonics are significantly off resonance which renders harmonic generation ineffective when $\delta n_a/n \lesssim .01$, the value that simulates the data best. Because an effective nonlinear model valid for CO_2 and Krypton plasmas does not exist in the literature, we will use a phenomenological model in the fluid simulations presented in Sec. V.

C. Stimulated Brillouin Back-Scattering Thresholds and Gains

The SBS amplitude temporal growth rate without including damping of either decay wave is

$$\gamma_0 = \frac{1}{8}\frac{V_0}{V_e}\sqrt{\frac{N_e}{N_c}}\sqrt{\omega_a\omega_0} \tag{8}$$

where $V_0 = eE_0/m_e\omega_0$ is the oscillatory velocity of the electron in the laser electric field, E_0. Typically, the strength of stimulated backscattering is discussed in terms of the gain factors that are the measure when the instability is convective. In the intermediate to high Z plasmas that are considered here, the ion wave damping is small enough that absolute growth is possible. To remind the reader, the parametrically coupled waves grow in time *convectively* at the rate $\sim \gamma_0$ to a finite final amplitude from an initial value in a frame moving at $(v_g - v_{ga})/2 \sim -|v_g|/2$ where v_{ga} is the ion acoustic wave group velocity. The

TABLE II: The convective and absolute intensity SBS thresholds for 4% N_c^{351}.

	$\lambda_0 = 351nm$		$\lambda_0 = 527nm$	
	$I^{cnv}(W/cm^2)$	$I^{abs}(W/cm^2)$	$I^{cnv}(W/cm^2)$	$I^{abs}(W/cm^2)$
CO_2	1.2×10^{12}	2.6×10^{15}	9.6×10^{11}	6.7×10^{14}
Kr	4.6×10^{12}	5×10^{15}	3.6×10^{12}	1.3×10^{15}

wave can also grow at a fixed point until nonlinear limits are reached if it is absolutely unstable but the intensity threshold for absolute growth is higher and the temporal growth rate γ_0^{abs} is smaller than γ_0 by the factor $\sqrt{|v_{ga}/v_g|}$. If the gain for convective growth is large enough, e.g. greater than 20, the convective interaction certainly will be nonlinear also. The damping thresholds for convectively unstable SBS in these weakly damped acoustic wave plasmas occur at low laser intensity. Convective and absolute growth occur if $\gamma_0 > \gamma_0^{cnv}$ and $\gamma_0 > \gamma_0^{abs}$ respectively where,

$$\gamma_0^{cnv} = \sqrt{\nu_a \nu_{ib}} \tag{9}$$

$$\gamma_0^{abs} = \frac{\sqrt{|v_{ga} v_g|}}{2}\left(\frac{\nu_a}{|v_{ga}|} + \frac{\nu_{ib}}{|v_g|}\right), \tag{10}$$

where $\nu_{ib} = 0.5 N_e \nu_{ei}/N_c = 0.5 v_g \kappa_{ib}$ is the light wave inverse bremsstrahlung absorption rate.

In Table II, the absolute and convective threshold intensities are evaluated for CO_2 and Krypton plasma parameters characteristic of the plateau region in the 4% fill. The convective SBS threshold is greatly exceeded for all conditions. The absolute threshold is exceeded only in the laser speckles for 351 nm illumination and is marginally exceeded for the nominal (vacuum) laser intensity for 527 nm light. However, the absorption of the laser light in the Krypton blast waves reduces the average laser intensity in the plateau region enough that the absolute threshold is also only exceeded in the laser speckles. Absolute growth in laser speckles would occur on timescales of the transit time of the sound wave along an f/6.7 speckle, namely 350ps for 351 nm light, during which time the speckle location will have changed and the plasma parameters as well.[29] Given that convective growth is certainly occurring in these plasmas, the convective gain exponent provides a good guide to the level of SBS that should be expected.

An approximate formula for the SBS intensity gain is[30]

$$G_{sbs} = \frac{1}{8}\frac{N_e}{N_c}\frac{V_0^2}{V_e^2}\frac{\omega_0}{c}Min(\omega_a L/\nu_a, \pi L_\nabla), \tag{11}$$

where ν_a is the amplitude damping rate of the acoustic wave, L is the plasma length, and L_∇ is the gradient scalelength of the dominant inhomogeneity, usually the velocity gradient but for $k\lambda_{de} \sim 1$, the density gradient is important. One sees from Eq. 7 that $\nu_a/\omega_a < .01$ for intermediate to large Z plasma and, for weak gradients, the SBS gain can be quite large (*e.g.* $G_{sbs} \sim 20$ in one speckle length, $L_s = 8f^2\lambda_0$, if the laser intensity is 8×10^{14}W/cm^2, the electron temperature is 3 keV, the electron density is $0.08N_c$) . Here, the focusing optic f-number is $f = 6.7$ for the Omega Laser Facility and λ_0 is the laser wavelength. Exterior to the blast waves, the flow velocity gradients ($L_\nabla \sim L_s$) limit the 351 nm light gain to less than one for the average intensity so little 351 nm SBS is expected from that region. On the other hand, the 527 nm light SBS gain is ~ 4 for the average laser intensity, $N_e/N_c^{527} = .04$, $T_e = 2.5$keV, and $L_\nabla = C_s/|\partial V/\partial z| = 0.25$mm, values typical for the lowest density fill near $V = 0$. For the higher density fills, this gain is achieved at points where $|V|$ is large enough to cause a significant Doppler shift.

The blast wave can absorb as much as 90% of the power of the 527 nm incident light at the higher Krypton fill densities. Thus, even if 100% of this power is reflected in the plateau, only 10% of that would be transmitted by the blast wave and measured by backscatter diagnostics as 1% reflectivity. Because transmission through the blast wave at the highest fill gas density is about 40% for 351 nm light, the SBS reflectivity could be as high as 16% at that density if we apply the same argument.

Before considering SBS gains in more detail, let's consider the possible influence of filamentation. The typical power in a speckle divided by the critical power for ponderomotively-driven filamentation is[30]

$$G_f = \frac{1}{4}\frac{N_e}{N_c}\frac{V_0^2}{V_e^2}\frac{\omega_0 L_s}{c}. \tag{12}$$

In the case of 527nm incident light, $L_s \sim 0.27$mm. If $G_f > 1$, the speckle will self focus.[31] In Fig. 9, this filamentation gain parameter given in Eq. (12) is shown as a function of the position in the $0.07N_c^{351}$ Krypton gasbag for incident 527nm laser light. This parameter is averaged over the length of a speckle. Because of the strong laser light absorption, this speckle self-focusing gain factor is bigger than one only in the expanding plasma which is itself only about a speckle length. For other Krypton fills, the behavior is similar. For

351nm incident light, filamentation is less important because the typical power in a speckle is smaller as $L_s \propto \lambda_0$ and $V_0 \propto \lambda_0$ for constant laser intensity. For CO_2 gasbags filled to 4% N_c^{351} and illuminated with 351 nm light this gain factor is ~ 1 over the entire length of the plasma. Note in the region of plasma where the SBS gain is dominated by gradients the filamentation gain given in Eq. (12) and the SBS gain in Eq. (11) are nearly the same if the speckle length is about the plasma scale length. That is the case considered here.

Localized pressure gradients induced by absorption of the nonuniform light intensity add to the ponderomotive force and increase the depth of the density perturbations when electron thermal conduction is not fast enough to smooth the temperature gradients. In the hot plateau region, for both Krypton and CO_2, the slowing-down mean free path $\lambda_e \sim \sqrt{Z}\lambda_{ei}$ is greater than 100/k with $k \sim \omega_0/2fc$ which is beyond the parameter range covered by the Fokker-Planck simulations.[32] On the other hand, the temperature in the plasma expansion low enough that $k\lambda_e \sim 10$ for which parameter, the thermal conduction is known to be reduced. This enhancement in filamentation gain is not sufficient to make 351 nm light filamentation unstable. However, filamentation for 527 nm light, including thermal effects on self-focusing [33], plays an important role in the pF3D simulations of SBS from high-Z Krypton plasmas.

In calculating the SBS gain, we use the more general formulation,

$$pG_{sbs}(\omega_s, z) = \int_{-\infty}^{z} dz \left(\frac{k^2 V_0^2}{8 v_{gs} \omega_s} Im \left(\frac{\chi_e (1+\chi_i)}{\varepsilon(\omega_0 - \omega_s, z)} \right) - \kappa_{ib}(\omega_s, z)/2 \right), \quad (13)$$

$$G_{sbs}(\omega_s) = pG_{sbs}(\omega_s, z_*), \quad (14)$$

that allows for re-absorption and ends the integration at the z_* for which $pG_{sbs}(\omega_s, z)$ is largest. The light is assumed incident from $z = -\infty$. In most cases, the peak gain corresponds to ~ 10 Å redshift for the 527 nm light and ~ 7 Å redshift for the 351 nm light. As displayed in Table III, the shift for peak gain of 351nm SBS is within an 1 Å of the experimental result shown in Table I and in Fig. 2. In the CO_2 gasbags the 351 nm gain is strongly peaked at ~ 7 Å for 351 nm light. Re-absorption is not a significant effect for CO_2 plasmas. Because the gain at other wavelengths is less than one for 351 nm light and the gain for speckle self-focusing is also, the good agreement is expected.

For 527 nm light the peak of the SBS gain has little correspondence with the measured spectral shift as seen in Table III. The two factors that explain the discrepancy are the filamentation gain parameter which is larger than one (see Fig. 9) and the SBS gain which

is ~ 4 in the expanding plasma for 527 nm light. Under these conditions, a few % SBS is likely from localized regions where the laser intensity is much higher than the average.

The peak SBS intensity gain as a function of the electron density of the fill gas is plotted in Fig. 10 for both 351 and 527 nm incident light. Also shown is the gain for 351nm light without accounting for the absorption in the blast wave or the additional gain in the expanding plasma. These two gains are nearly the same for the lowest fill density. For the higher density fills the gains without the blast wave absorption are higher. The factor $(N_e/V_e^2)\omega_a L/\nu_a$ in Eq. (11) is nearly the same for 527 and 351 nm light. If the absorption were weak, one would expect a $\lambda_0^3 \sim 3$ scaling of the gain from the remaining factors. However, the gains in Fig. 10 for incident 351nm and 527nm for the same gasfill do not obey that scaling. Including blast wave transmission from Fig. 7, one expects the 527 nm light SBS gain to be twice that of 351nm at 4% N_c^{351} but only 70% at 11% N_c^{351} in agreement with the gain scaling in Fig. 10.

Again the gains are lower at the higher fill gas density because of the stronger absorption of the laser light in the higher density blast waves of the higher density fills. The 351 nm gain shows an increase with fill gas density as one expects from Eq. (11) until absorption in the blast wave comes into play at the highest fill density. The 527 nm gain is highest at the lowest fill density because blast wave absorption is minimized. The SBS gain is largest and varies little during the first half of the interaction pulse. After the heaters turn off during the second half of the interaction pulse, the electron temperature decreases, absorption of the interaction pulse increases, the length of the plateau region decreases, and, consequently, the gain decreases.

D. Stimulated Raman Back-Scattering Gains

The SRS gains for 527nm incident light must take into account the presence of the blast waves because, as one can see from Fig.5, the peak density of the blast wave may exceed the critical density for the SRS light amplified in the density plateau between the blast waves. For the cold plasma Langmuir wave frequency, the SRS scattered light frequency from the plateau density in the $.07N_c^{351}$ fills is almost exactly equal to the maximum plasma frequency in the blast wave; that is, the SRS light would be internally reflected. With the increase in the Langmuir wave frequency from the thermal dispersion, this reflection is

TABLE III: The measured SBS spectral shift and the spectral shift corresponding to the peak of the SBS gain

		$\lambda_0 = 351$ nm		$\lambda_0 = 527$ nm		
N_e/N_c^{351}	Gas	$\Delta\lambda_0^{expt}(\mathring{A})$	$\Delta\lambda_0^{th}(\mathring{A})$	$\Delta\lambda_0^{expt}(\mathring{A})$	$\Delta\lambda_0^{th}(\mathring{A})$	Omega Shot number
.05	CO_2	8	7	3	11	27692
.05	Kr	5.5	6	1.4	10	29676
.06	Kr	6.5	7	-	10	32053[a]
.07	Kr	7	7	1.4	11	29674
.09	Kr	7.5	-	-1	-	29678
.11	Kr	-	7	-	-5:10	-

[a]There was no 527 interaction beam because this shot had Thomson scattering which uses the same beamline.

assured. For the higher density fills, the plateau density is about $1/4N_c$ which ensures that any SRS scattered light will not escape the plasma. The Langmuir waves in the plateau region are weakly damped for higher density fills and strongly damped for lower density fills as $k_{lw}\lambda_{de} = 0.37, 0.29, 0.23$ for $N_e/N_c^{351} = .04, .06, .08$ respectively. Here, k_{lw} is the wavenumber of the Langmuir wave. Although the SRS light may not escape the plasma, the SRS of 527nm light in the plateau region might be significant enough to reduce the SBS by competition. However, simulations (discussed in Sec. V) with both SBS and SRS did not show any reduction in SBS in the most likely case where $k_{lw}\lambda_{de} = 0.3$. Thus the SRS gains for the 527nm incident light can be calculated for the expanding plasma outside the blast waves where laser absorption is not important. The 527 nm gains are a few in the expanding plasma outside the blast wave. Significant growth, leading to about 1% SRS can occur localized in speckles, but simulating that effect requires a good representation of high intensity speckles by large 2D or 3D regions. Since SRS plays a minor role in the energetics of these plasmas, such simulations were not pursued.

For the 351nm incident light, internal reflection of the light SRS scattered from the plateau does not occur but significant inverse bremsstrahlung re-absorption needs to be included to estimate the backscattered SRS. For the higher density fill, the peak density in

the blast wave is above $N_c/4$ and the SRS spectrum will extend up to $\sim \lambda_0/2$. Because of the quarter-critical density, the $2\omega_{pe}$ instability, which we do not consider here, is also possible in these plasma. The peak density in the blast wave for the lower density fill is less than quarter-critical density for 351nm light. The 351nm SRS gains are insignificant because the Langmuir wave in the plateau region is strongly damped or nonresonant ($k_{lw}\lambda_{de} = 0.6, 0.47, 0.4$ for $N_e/N_c^{351} = .04, .06, .08$ respectively).

V. TWO DIMENSIONAL SIMULATIONS OF LIGHT PROPAGATION AND STIMULATED BRILLOUIN BACK SCATTER

The simulation code pF3d[34] was used to propagate self-consistently the incident light through the Krypton and CO_2 plasmas. Here the small-scale structure of the laser beam, speckles, and the overall spot size are taken into account. In addition to ponderomotive self-focusing, enhanced focusing from thermal pressure gradients computed with a nonlocal heat conductivity are included. Backscattered SRS and SBS grow throughout the plasma from small amplitude fluctuations in the acoustic waves and Langmuir waves with the effects of light reabsorption naturally included. As mentioned previously, little self-focusing occurs for 351 nm light in these simulations of Krypton plasmas because the power in the 351 nm speckles is below threshold for self-focusing. In Fig. 11, two dimensional pictures of the simulated laser propagation through a Krypton-gas-filled bag is shown for 527nm and 351nm light. The 351nm light propagates with little spray but noticeable absorption in this example. The 527nm light is more strongly absorbed and shows some spray after propagating through the blast wave at which point there is little laser power left.

A. CO_2 plasma modeling

Because pF3D is a fluid code with enveloped equations for the light and SBS-driven acoustic waves, nonlinear limits on the growth of the acoustic waves must be imposed with models based on theory or kinetic simulations. A phenomenological model for limiting the acoustic wave amplitude was used previously for modeling SBS in CO_2 gasbags.[7] In this model, the damping on the acoustic wave is proportional to $|\delta \mathrm{n_{ac}}/\mathrm{n_{th}}|^{\mathrm{M_{nl}}}$ where $\delta \mathrm{n_{ac}}$ is the amplitude of the acoustic wave that backscatters the incident light, $\mathrm{n_{th}}$ is a fraction of local

electron density, and M_{nl} is typically 4. Using that model for the 4% fill CO_2 plasma with $n_{th} = .01 n_e$ produces a reflectivity of $\sim 20\%$ for 351nm incident light in reasonable agreement with the measured 25% 351 nm reflectivity. Without limits, the CO_2 351 nm SBS simulated reflectivity is $\sim 55\%$.

In these simulations, good agreement with the measurements of total SBS was found for both laser wavelengths and for Krypton and CO_2 fills if the amplitude of the ion acoustic waves was limited to 1% of the local electron density. This value is significant bigger than the value needed in previous simulations of the 351 nm reflectivity from CO_2 gasbags at the NOVA laser facility.[7] There are several differences between those simulations and the current ones. In Ref. [7], only the plateau was simulated, the plasma parameters were $N_e = 0.065 N_c^{351}$, $T_e = 2.7\text{keV}, T_i = 1.5\text{keV}$, the mean velocity $< \mathbf{V} >= \mathbf{0}$, and the laser beam envelope was uniform in the transverse dimension. For a plateau length of 1.7mm with uniform density, temperature, and no flow, the linear SBS intensity gain is 350, an order of magnitude larger than the CO_2 gains for the OMEGA gasbags. For this more unstable case, the pf3d simulated reflectivity is 85% without limits on the acoustic wave, 72% if the acoustic wave limit is 1%, and 20% if the limit is 0.2% which is the limit used in Ref. [7]. Thus, less stringent limits on the acoustic wave amplitude are required if the self-consistent plasma profiles with gradients in the electron temperature, density, and flow velocity are used.

B. Krypton plasma modeling

1. 351 nm light scattering

In agreement with the gain calculations presented in the previous sections, SRS is much smaller than SBS. In the simulations without any nonlinear limits (other than pump depletion), the SBS reflectivity is $\sim 20\%$ for 351nm light for fill densities between $.04 - .08 N_c^{351}$ for plasma conditions computed by HYDRA 900 ps after the heater beams turned on. The time-averaged SBS reflectivity into the FABS detector at OMEGA is about ten times smaller. If there were much SBS that was scattered outside the FABS detector, this calculation might be within the error of the measurement. However, the calculations do not support such an interpretation as there is little self-focusing of the incident light that would cause backscatter

at angles outside the FABS. The simulation predicts more than 80% within the FABS.

Using the same phenomenological model for these Krypton gasbags that was used for CO_2 bags, we find that SBS is strongly reduced. With the 1% limit on the acoustic wave amplitude at all Krypton fill densities, the computed SBS reflectivity agrees reasonably well with the time-average measurements as shown in Fig. 12. The simulated reflectivity increases with gas-fill density in part because the nonlinear limit on the acoustic wave amplitude is proportional to the local electron density. A different nonlinear model might show different scaling behavior.

2. 527 nm light scattering

For 527nm light, the SBS reflectivity without limits on the acoustic wave amplitude decreases from about 15% at the lowest fill density to about 8% at the higher fill densities as shown in Fig. 13. This trend is presaged by the variation of the 527 nm gain with fill density at constant laser power shown in Fig. 10. The actual laser power for the $4\%N_c^{351}$ shot was about 30% of the other shots and the pF3d simulation was done with the actual power. When the acoustic wave amplitude is limited with the same model as with the 351 mn light, the SBS reflectivity is decreased at all densities and is in good agreement with the time-average data. However, when one compares the simulated spectrum of the scattered light to the measured spectrum, the agreement for 527 nm light is not very good because the simulated shift corresponds with the peak of the gain whereas the measured spectral peak does not (see Table III). The measured 527 nm reflectivity at the shift corresponding to the peak gain is much smaller than the simulated one. Moreover, the simulated reflectivity at the shift corresponding to the peak of the measured spectra is too small. The most likely resolution of both discrepancies is the same, three dimensional simulations that correctly include the power in intense speckles which would simultaneously increase the SBS in the expanding plasma and cause the incident light to spray. The spraying has the additional effect of lowering the intensity in the plateau and reducing the SBS there. In Sec. VI, a few three dimensional simulations of 527 nm light propagating through the plasma expansion will test this *ansatz*.

3. interpretation of 351 nm SBS simulations

The time dependence of the 351 nm light reflectivity and transmission predicted by the pf3d simulations for the lowest density Kr fill is shown in Fig. 14 for a interaction beam pulse that turns on instantly at 0.5 ns and has constant power for 1 ns. The transmission increases as the electron temperature increases and the length of the plateau decreases with time until the heater beams turn off. After that time, the electron temperature decrease increases the absorption. The model developed for the SBS reflectivity from CO_2 gasbags at Nova where the acoustic wave amplitude was nonlinearly "clamped" at amplitude n_d was $R = [0.88\omega_0 L n_d/4 v_g n_c]^2$ where L was the plasma plateau length.[7] This formula is valid in the plateau since, for 351 nm light, the absorption length $L_a = c/(n_e\nu_{ei}/n_c) > L$. The reflectivity slowly decreases as the length of the gain region, L, decreases. In pf3d simulations, it takes ~ 100 ps for the SBS to reach a saturated value but the reflectivity is plotted at the time that the HYDRA plasma parameters are valid. The actual incident laser interaction pulse, a typical one is shown in Fig. 2, takes 200 ps to reach full power. These effects and the detector response time can explain the difference between time dependence of the pf3d simulated reflectivity and the measured reflected power.

For the simulation parameters that best match the data, the influence of the blast wave absorption on the reflectivity is examined by computing the reflectivity of the plateau region as the ratio of the reflected light before transmission through the blast wave to the incident light after transmission through the blast wave. This "plateau" reflectivity is compared with the the ratio of the reflected light to the incident light in Fig. 15. At low density the difference between these two reflectivities is small. As the fill density increases, the differences increase. For 527 nm light most of the reflectivity at the higher density comes from the expanding plasma region where the intensity is highest. For 351 nm light, on the other hand, the reflectivity is higher computed inside the plasma than outside because absorption of the reflected light in the blast wave is more important than the extra gain experienced by the reflected light in the expanding region.

The blast wave absorption is not the sole reason that the 351 nm light reflectivity is small in Krypton plasmas. To examine other reasons, the reflectivity from a 7% Krypton fill is examined in detail. First, a simulation with a uniform density of $.065 N_c^{351}$ and a uniform electron temperature of 4 keV with a incident laser beam of intensity $8 \times 10^{14} W/cm^2$ is

considered with the 1% limit on the acoustic wave imposed. Nearly seventy percent of the light is reflected. Even if the incident intensity is lowered to $5 \times 10^{14}\mathrm{W/cm^2}$ to account for the 40% absorption in the blast wave, the plateau reflectivity is 60-65%. With account of the absorption of the backscattered light in the blast wave, the predicted reflectivity from this calculation would be smaller, 22%, but still higher than measured. If the actual plasma parameter profiles of the Hydra simulations without the blast waves are used, the plateau reflectivity drops to 25-30% which would still project to a larger reflectivity, namely 9-11%, than measured or simulated when the Hydra profiles with the blast waves are included, namely 3-5%. The last ingredient that lowers the reflectivity to the full simulation value is the temporal incoherence acquired by the laser beam as it propagates through the expanding plasma and the blast wave before it enters the plateau region where backscatter occurs. When one simulates this laser light incoherence by using a model of SSD with $1\mathring{A}$ of bandwidth at 351 nm, the "plateau" reflectivity is 10% which agrees with the full simulation value of 3.6% when the blast wave absorption is accounted for.

With the imposed SSD, the simulations showed that the backscatter is less phase correlated with the incoming light (than without SSD) within a few hundred wavelengths of the simulation boundary, that is, within the first speckle length. The reflected light and the associated acoustic wave also grow less rapidly over this length in the full simulation and in the simulation with imposed SSD (than in the simulation without SSD).

VI. THREE DIMENSIONAL SIMULATIONS OF SBS IN EXPANDING PLASMA

The 2D simulations of the 351nm SBS from both Krypton and CO_2 plasma showed the spectral redshift of $\sim 7\mathring{A}$ expected from the gain calculations. However, the 2D simulations of the 527nm SBS from Krypton plasmas differed from the data in two respects that are resolved by 3D simulations. The two differences are that the model shows a gradual decrease of SBS with gas fill density and a redshift of 10 Å while the data shows an increase of SBS and a redshift that decreases with gas fill density. The latter difference is a more important problem to address because it calls into question the value of the gain as a predictor of reflectivity. The key differences between 351nm and 527nm light propagation are the gains for SBS and filamentation are greater than one only for 527nm light in the plasma flowing opposite to the laser propagation direction. Because of the strong velocity gradient and

the weak linear damping, the SBS in this region occurs in a distance less than a speckle (hotspot) length. Thus the theory of stimulated backscatter by independent hot spots is applicable in which the reflectivity of each hotspot is averaged over the distribution function of hotspot intensities.[37] The SBS reflectivity becomes $R \sim \int dI R(I)P(I)$ where R(I) is the reflectivity of the hotspot of intensity I and P(I) is the probability distribution. In the case considered here where the gain for the average intensity is ~ 4, strong SBS is expected for hotspots with intensity more than $5\times$ the average where about 4% of the incident beam energy resides. This 1D independent-hot-spot model has been improved by consideration of mitigating effects of diffraction and gain narrowing[38] both of which lower the reflectivity of the individual hotspot. These effects are naturally included in pF3d simulations.

Because self focusing of the speckles is transferring power to higher intensity, the amount of power available for strong SBS is increased. Because the 2D simulations under-populate the distribution of hotspots with higher than average intensity, filamentation and SBS in the plasma expansion are weaker in 2D than 3D. In Fig. 16, the distribution of intensities from 2D and 3D pF3d simulations for the conditions pertinent to 7% Kr fill at 900 ps are shown that confirm these assertions. The transverse size and resolution of the simulation are the same for 2D and 3D but the number of speckles in 3D is far greater. The figure shows that our 2D simulations under-represent the power at high intensity and that speckle self focusing significantly increases the power at intensities more than $5\times$ the average intensity. In this example, only ponderomotive self focusing was included. For the transverse wavenumber typical of the incident beam speckles, $k = k_0/2f$, the electron slowing down mean free path, λ_e, satisfies $k\lambda_e \sim 10$ which is in the range where thermal self focusing will enhance the focusing.

In these simulations, the SBS reflectivity was 2-10 % with a wavelength shift of the scattered light from the incident light, $\Delta\lambda = \lambda_s - \lambda_0 \sim 2 - 5\mathring{A}$ where amount of scatter and wavelength shift depended on the strength of self-focusing and the nonlinear limits on the acoustic wave. With self focusing turned off by neglecting light refraction, the total reflectivity was $R = 2\%$ and the shift was $\Delta\lambda = 6\mathring{A}$. With only ponderomotive focusing (the case shown in Fig. 16), $R \sim 7\%$ and the shift was $\Delta\lambda = 4\mathring{A}$ with a FWHM of 6 Å. Most of the reflected light is not confined to the incident light cone. The light reflected into the solid angle of the incident light is 0.1% and 0.35% respectively. The backscatter of the light into a large solid angle is partly explained by diffraction after gain narrowing (the gain

is larger for light at the center of the spot) but mostly by the fact that the linear gain spatial resonance width ($\sim \pi\nu_a \mathrm{L_v}/\omega_\mathrm{a} \sim 6\times10^{-4}$cm) is so small that light scattered by up to 30° will be fully amplified.

In the simulations discussed in the previous paragraph, the acoustic wave was not nonlinearly limited. With ponderomotive self focusing and a nonlinear limit of $0.1\mathrm{N_e}$, the total reflectivity is 5% with 1% backscattered into the solid angle of the incident light and a wavelength shift of $5\mathring{A}$. This result is close to the experimental result in Fig. 4 but the redshift is bigger than the measured shift of 1.4Å given in Table I. With the addition of thermal self focusing to ponderomotive, enough power is concentrated in high intensity hotspots that 8% SBS occurs at a lower density where the Doppler shift to the blue is bigger ($\Delta\lambda \sim 2-5\mathring{A}$). With a nonlinear limit on the acoustic wave, the SBS backscattered light is confined within a small solid angle such that 2% of the incident light (1/4 of the total SBS) is backscattered within the incident light cone angle.

One nonlinear effect that might limit the SBS reflectivity is a nonlinear frequency shift of the acoustic wave. Nonlinear ion frequency shifts in this case where the phase velocity is much larger than the ion thermal speed are negligible. Electron nonlinear frequency shifts lead to a higher frequency acoustic wave and thus a bigger redshift in the scattered light and a bigger difference between the modeling and the measurement.

As a further check on our modeling, we simulated in 3D the propagation of 527 nm light without nonlinear limits on the acoustic wave through the expanding plasma of a C_3H_8 gasbag filled to $.065N_c^{351}$. Because the C_3H_8 acoustic wave damping is 10× larger than that for CO_2, the resonance width is $\sim$ 0.06cm which is comparable to the initial speckle length. The linear gain is similar to that for Krypton and CO_2 in this region because the velocity gradient is the dominant factor limiting the gain. The simulations show insignificant SBS because filamentation reduces the speckle length to less than the resonance width so that gain is averaged over several speckles. This result agrees with the C_3H_8 experimental measurements of SBS spectra from gasbags.

It remains to explain why the SBS from the plateau is weaker experimentally than in the 2D simulations. Filamentation and stimulated *forward* SBS of the 527 nm light provide the answer. The 3D simulations of 527 nm light propagation in 7% Kr fill at 900 ps with thermal effects included show the beam focuses in the region where the flow is nearly sonic ($V_{flow} \sim 3\times10^7$cm/s) and then sprays into a f/2.5 cone as it propagates to the region where

the flow reverses direction ($V_{flow} = 0$). Then it is strongly absorbed by the blast wave. This spray was modeled in 2D by propagating an f/2.5 beam through the blowoff plasma, the blast wave, and the plateau with its focus where the beam sprays in the 3D simulations. The total SBS from this simulation is 1% but it is spread over the f/2.5 cone angle. The SBS into the FABS (what is measured in the experiment) from this calculation is 0.1%, much smaller than the 3% from the 2D simulations that did not account for beam spray and in better agreement with the data.

VII. CONCLUSIONS

We have explained why the SBS is lower for high-Z gas fills than for CO_2 fills of similar densities and temperatures with the same laser illumination. An *ad hoc* nonlinear limit on the acoustic wave amplitude was needed in both CO_2 and Krypton plasmas to reproduce the actual reflectivity values but its form was simple and independent of charge state.Nonlinear effects such as frequency detuning from electron trapping, two-ion wave decay, or generation of ion acoustic wave harmonics may be the nonlinearities responsible [8, 23] for keeping the ion wave amplitudes lower than linear theory with pump depletion. In these simulations, the best agreement with the measured reflectivity required a limit of 1% on the amplitude of the acoustic wave which is smaller than the linear threshold for two-ion wave decay by factor of 2-4. This threshold depends on the value of the electron Landau damping used. Kinetic nonlinearity may lower this value if the bounce frequency of an electron trapped in the acoustic wave satisfies $\omega_{Be} > \nu_{Le}$ which occurs for very small values of the acoustic wave amplitude. Here, ν_{Le} is the linear electron Landau damping rate for a Maxwellian plasma. The trapping of electrons also leads to a nonlinear frequency shift[27, 36] that might detune the SBS resonance in a similar manner to the ion trapping induced frequency shifts simulated [8, 9] and measured.[21]

This analysis shows that the nonlinear physics determining the amount of SBS when $ZT_e/T_i \gg 1$ is probably the same for CO_2 plasmas as it is for high Z plasma such as gold and Krypton because one can successfully model the SBS reflectivity of CO_2 and Krypton filled gasbags over a wide range of density and two different laser wavelengths with the same imposed limit on the acoustic wave amplitude. The lower than CO_2 measured SBS reflectivity from Krypton and Xenon-filled gasbags is primarily a result of strong inverse

bremsstrahlung in high-Z plasmas.

By detailed analysis of the 2D simulations of the 351 nm propagation, we showed that induced temporal incoherence on the laser beam also plays a role in modeling the SBS. The laser light acquires this incoherence by propagating through a time-varying, expanding plasma and blast wave where the SBS backscatter rate is small before encountering the plateau region where the strong backscatter occurs. Also of some importance in controlling SBS of 351 nm light in the plateau region are the temperature and density gradients which are calculated by the radiation-hydrodynamic code, HYDRA.

The 2D simulations of the 527 nm light propagation were misleading because they underestimate the amount of filamentation and beam spray. As a result the calculated amount of SBS in the blowoff plasma is too small and the amount from the plateau is too large. The 3D simulations model the SBS spectrum and the reflectivity well. This modeling also shows the need, when analyzing NIF ignition designs, of considering the effect on the incident light properties of the propagation through the intervening plasma and the role of self focusing in increasing the power at high intensity.

Acknowledgments

We acknowledge with pleasure stimulating discussions with W. L. Kruer and E. A. Williams. This work was performed under the auspices of the U.S. Department of Energy by the University of California, Lawrence Livermore National Laboratory under contract No. W-7405-Eng-48.

---

[1] J. A. Paisner, E. M. Campbell, and W. J. Hogan, Fusion Tech. **26**, 755 (1994)

[2] E. M. Campbell, J. T. Hunt, E. S. Bliss, D. R. Speck, and R. P. Drake, RSI **57**, 2101 (1986)

[3] S. H. Glenzer, R.L. Berger, L.M. Divol, R. K. Kirkwood, *et al.*, Phys. Plasmas **8**, 1692 (2001); S. H. Glenzer, L. J. Suter, R.L. Berger, K. G. Estabrook, *et al.*, Phys. Plasmas **7**, 2585 (2000); S. H. Glenzer, L. J. Suter, R. E. Turner, B. J. MacGowan, *et al.*, Phys. Rev Lett. **80**, 2845 (1998)

[4] S. H. Glenzer, L.M. Divol, R.L. Berger, C. Geddes, *et al.*, Phys. Rev Lett. **86**, 2565 (2001)

[5] J. M. Sources, *et al.*, Fusion Technol. **30**, 492 (1996)

[6] K. B. Fournier, C. Constantin, C. A. Back, L. J. Suter, *et al.*, "Electron density scaling of conversion efficiency of laser energy into L-shell X-rays," JQSRT in press

[7] L. Divol, R. L. Berger, B. I. Cohen, E. A. Williams, A. B. Langdon, B. F. Lasinski, D. H. Froula, and S. H. Glenzer, Physics of Plasmas **10**, 1822 (2003)

[8] B. I. Cohen, B. F. Lasinski, A. B. Langdon, and E. A. Williams, Physics of Plasmas **4**, 956 (1997); B. I. Cohen, L. Divol, A. B. Langdon, and E. A. Williams, Physics of Plasmas **12**, (2005)

[9] L. Divol, B. I. Cohen, E. A. Williams, A. B. Langdon, and B. F. Lasinski, Physics of Plasmas **10**, 3728 (2003)

[10] A.J. MacKinnon, S. Shiromizu, G. Antonini, J. Auerbach, *et al.*, Rev Sci Instrum **75**, 3906 (2004)

[11] The delay of the probe beam was imposed by strong plasma background radiation during the first 500 ps.

[12] M. M. Marinak *et al.*, Phys. Plasmas **8**, 2275 (2001)

[13] R. M. More, K. H. Warren, D. A. Young, and G. B. Zimmerman, Phys. Fluids **31**, 3059 (1988)

[14] W. A. Lokke and W. H. Grasberger, Lawrence Livermore National Laboratory internal report UCRL-52276 (1977)

[15] N. B. Meezan, L. Divol, M. M. Marinak, G. D. Kerbel, *et al.*, Phys. Plasmas **11**, 5573 (2004)

[16] S. Prisbrey, L. J. Suter, and N. Meezan, "Hydrodynamics of Blast Waves in LPI Gasbags," BAPS **50**, 110 (October 2005)

[17] R. London and M. D. Rosen, Physics Fluids **29**, 3813 (1986)

[18] The total intensity from the $39-42$ 351nm heater laser beams that that are focussed far from the target center and illuminate the bag from different angles peaks in the bag center. [See Fig. 1 for the heater beam configuration.]

[19] C. J. Randall, Phys. Fluids **25**, 2231 (1982)

[20] M. D. Tracy, E. A. Williams, K. G. Estabrook, J. S. DeGroot, S. M. Cameron, Phys. Fluids B **5**, 1430 (1993)

[21] D. H. Froula, L. Divol, H. A. Baldis, R. L. Berger, *et al.*, Phys. Plas. **9**, 4709 (2002)

[22] S. J. Kartunen and R. R. E. Salomaa, Physics Lett. **72A**, 336 (1979)

[23] C. Riconda, A. Heron, D. Pesme, S. Huller, *et. al.*, Phys. Rev. Lett. **94**, 055003 (2005)

[24] D. Pesme, C. Riconda, V. T. Tikhonchuk, Phys. Plasma **12**, 092101-1 (2005)

[25] C. Niemann, S. H. Glenzer, J. Knight, L. Divol, *et al.*, Phys. Rev. Lett. **93**, 035002 (2004)

[26] S. J. Kartunen and R. R. E. Salomaa, Physics Lett. **88A**, 350 (1982)

[27] R.L. Dewar, W. L. Kruer, and W. M. Manheimer, Phys. Rev. Lett. **28**, 215 (1972)

[28] C. Riconda, A. Heron, D. Pesme, S. Huller, *et al.* Phys. Plas. **12**, 112308-1 (2005)

[29] The simulations discussed in Sec. V include both convective and absolute instabilities.

[30] J. D. Lindl, P. Amendt, R. L. Berger, S. G. Glendinning, *et al.*, Phys. Plasmas **11**,339 (2004)

[31] E. A. Williams has shown that this parameter provides a good guide to the onset of self-focusing and beam spray.

[32] E. Epperlein, Phys. Rev. Lett. **65**, 2145 (1990)

[33] The algorithms in pf3d were revised in 1997 such that the linear hydrodynamics used in prior publications was replaced by nonlinear hydrodynamics. In the process, the description of nonlocal transport was changed from that described in T. Kaiser, *et al.*, Phys. Plasmas **1**, 1287 (1994) to the one described in Reference ([34]). In both descriptions, the nonlocal heat conduction is reduced less than the extrapolation of the results in Ref. ([32]) if $k\lambda_{ei} > \sqrt{Z}$. With this *ad hoc* formulation, pf3d simulates the measured angular distribution of transmitted light well.

[34] R. L. Berger, C. H. Still, E. A. Williams, and A. B. Langdon, Physics of Plasmas **5**, 4337 (1998)

[35] C. Niemann, L. Divol, D. H. Froula, G. Gregori, *et al.*, Phys. Rev. Lett. **94**, 085005 (2005)

[36] Vlasov simulations of large-amplitude ion acoustic waves with $C_s \gg V_{ti}$ have confirmed the electron trapping frequency shift calculated in Ref. ([27]); S. Brunner, private communication 2005.

[37] H. A. Rose and D. F. DuBois, Phys. Rev. Lett. **72**, 2883 (1994)

[38] L. Divol and P. Mounaix, Phys. Plasmas **6**, 4037 (1999)

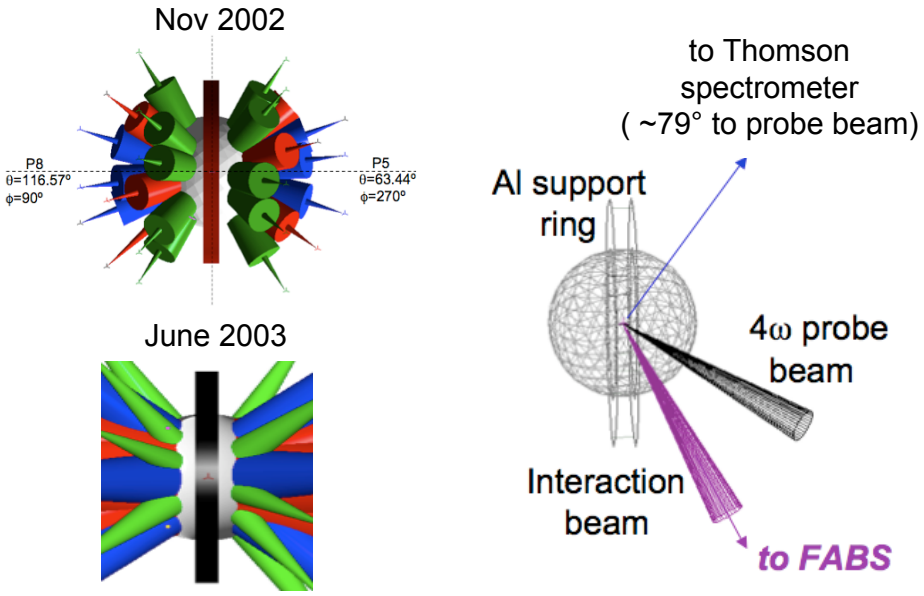

FIG. 1: The experimental setup for the Krypton-filled gasbag targets shot in Nov 2002 and June 2003 at the Omega Laser Facility

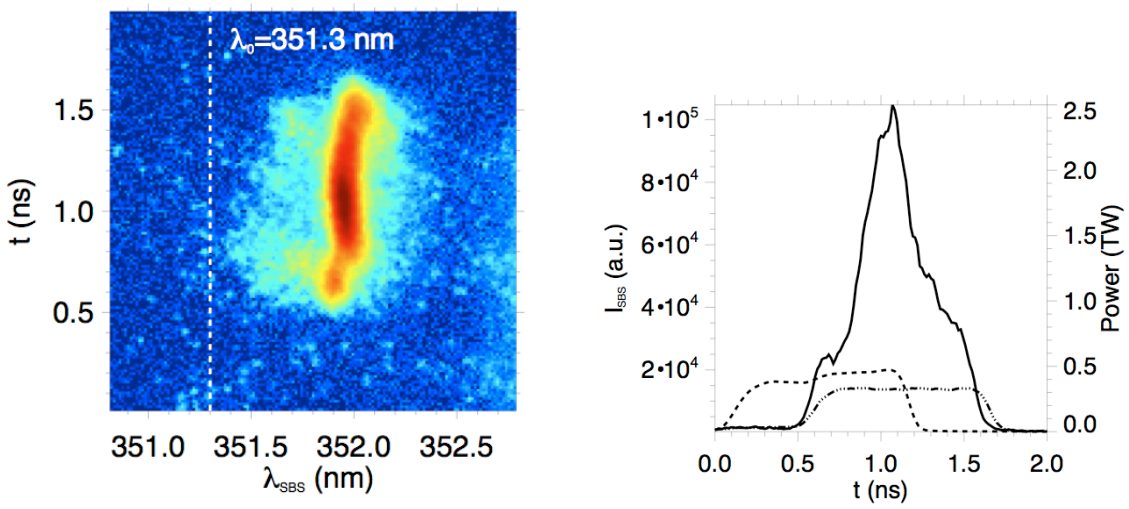

FIG. 2: 351nm SBS spectra from the $0.06N_c^{351}$ target. (*left*) The SBS streak spectra and (*right*) the time dependence of the heater beams (dots), the 351nm interaction beam (dash-dot), and the SBS backscatter (solid). The SBS light is redshifted by $6.5\mathring{A}$ from the interaction beam.

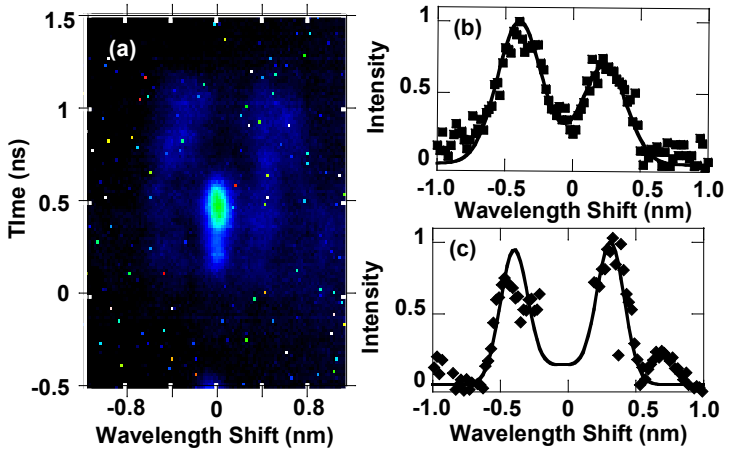

FIG. 3: Thomson scatter streaked spectra from the $0.06N_c^{351}$ target. (a) The TS streak spectra, (b) the spectrum at 1.2 ns (squares) and a fit ($T_e = 2$keV) to the spectrum (solid line), and (c) the spectrum at 0.5-0.8 ns (squares) and a fit ($T_e = 3.5$keV) to the spectrum (solid line). The bright unshifted light is stray light.

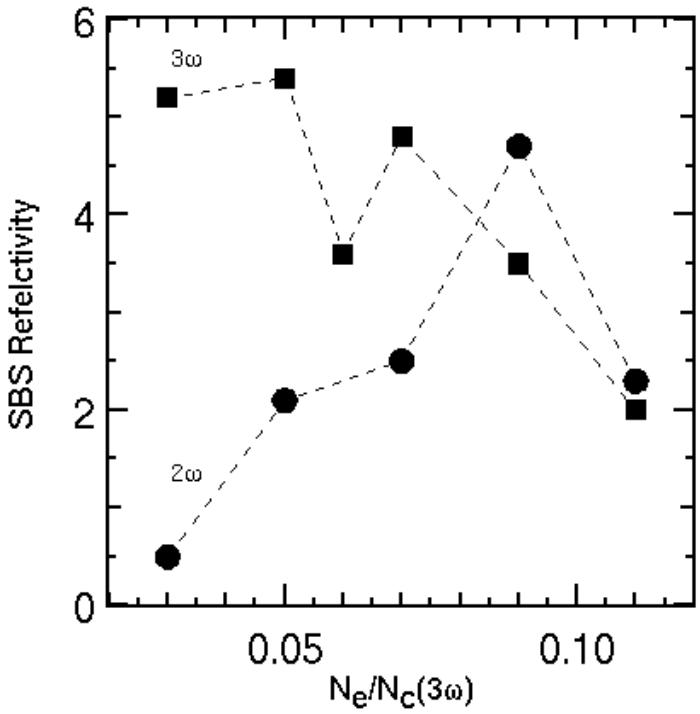

FIG. 4: The time integrated SBS from Krypton gas filled targets as a function of the electron density of the fiil in units of the 351 nm critical density for 527 nm and 351 nm interaction beams. The 351 nm data at $.06N_c^{351}$ is from a June 2003 shot which used a different heater beam configuration. The interaction beam power of the lowest density 527 nm shot was about 1/3 of the rest of the shots.

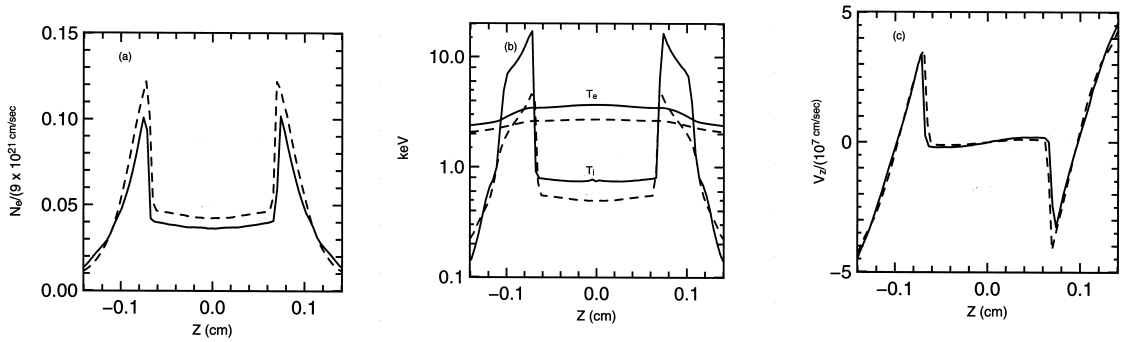

FIG. 5: The plasma electron density (a), the electron and ion temperatures (b), and the axial flow velocity (c) for the $4\%N_c^{351}$ Krypton fill (solid lines) and for the $4\%N_c^{351}CO_2$ fill (dashed lines) at 900ps into the 351nm wavelength heater laser pulse.

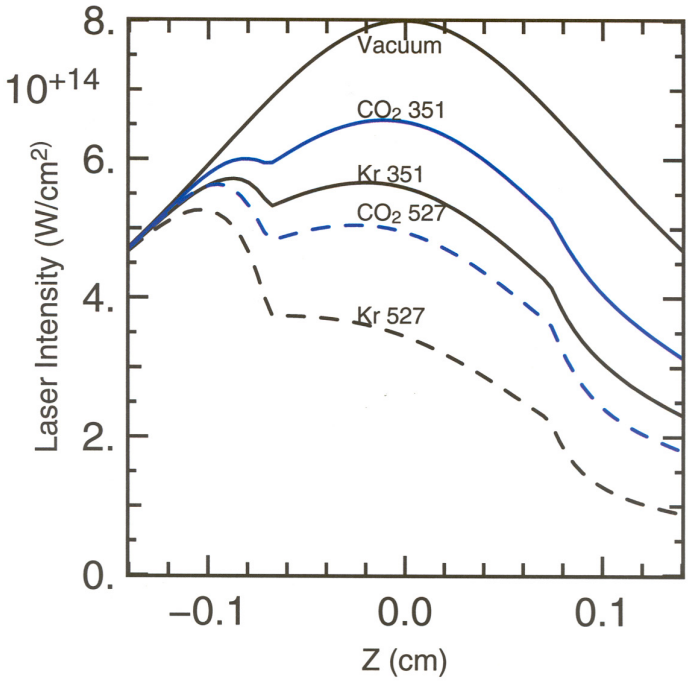

FIG. 6: The laser intensity focused at $z = 0$ vs distance into the bag for a 527nm laser beam into a 4% Krypton fill, a 351nm laser beam into a 4% Krypton fill, a 527nm laser beam into a 4% CO_2 fill, and a 351nm laser beam into a 4% CO_2 fill. The vacuum laser intensity at focus is $8 \times 10^{14}\mathrm{W/cm^2}$.

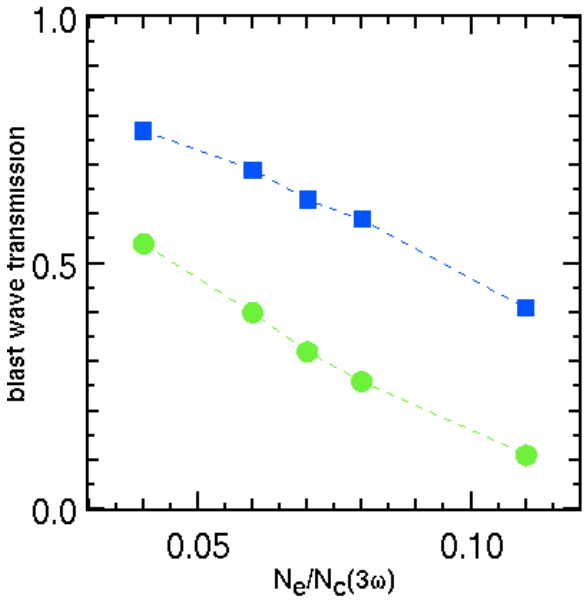

FIG. 7: The laser power transmission through the blast wave as a function of the electron density in units of the 351nm critical density for 351nm (blue squares) and 527 nm (green circles) incident laser light.

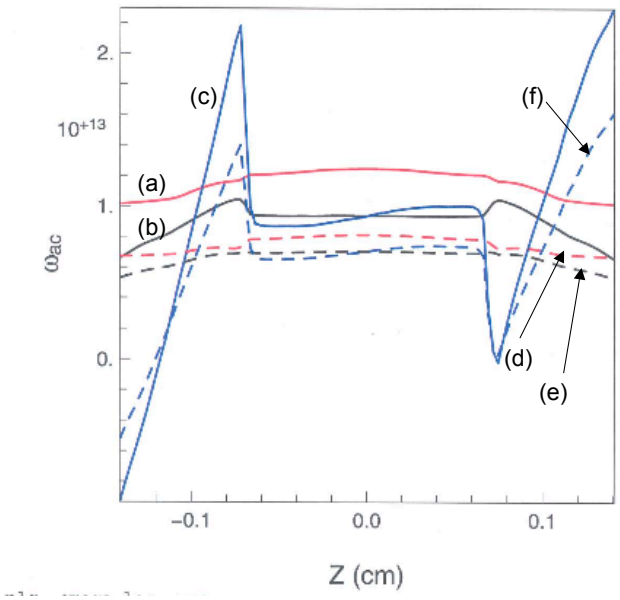

FIG. 8: The local acoustic wave frequency for the Krypton 4% N_c^{351} gasbag at 900ps as a function of z for the 351nm wavelength interaction beam and (a) when $k\lambda_{de}$ is not included in the dispersion, (b) when $k\lambda_{de}$ is included in the dispersion, and (c) when the Doppler shift of the flow is included and for the 527nm wavelength interaction beam when (d) $k\lambda_{de}$ is not included in the dispersion, (e) $k\lambda_{de}$ is included in the dispersion, and (f) when the Doppler shift of the flow is included.

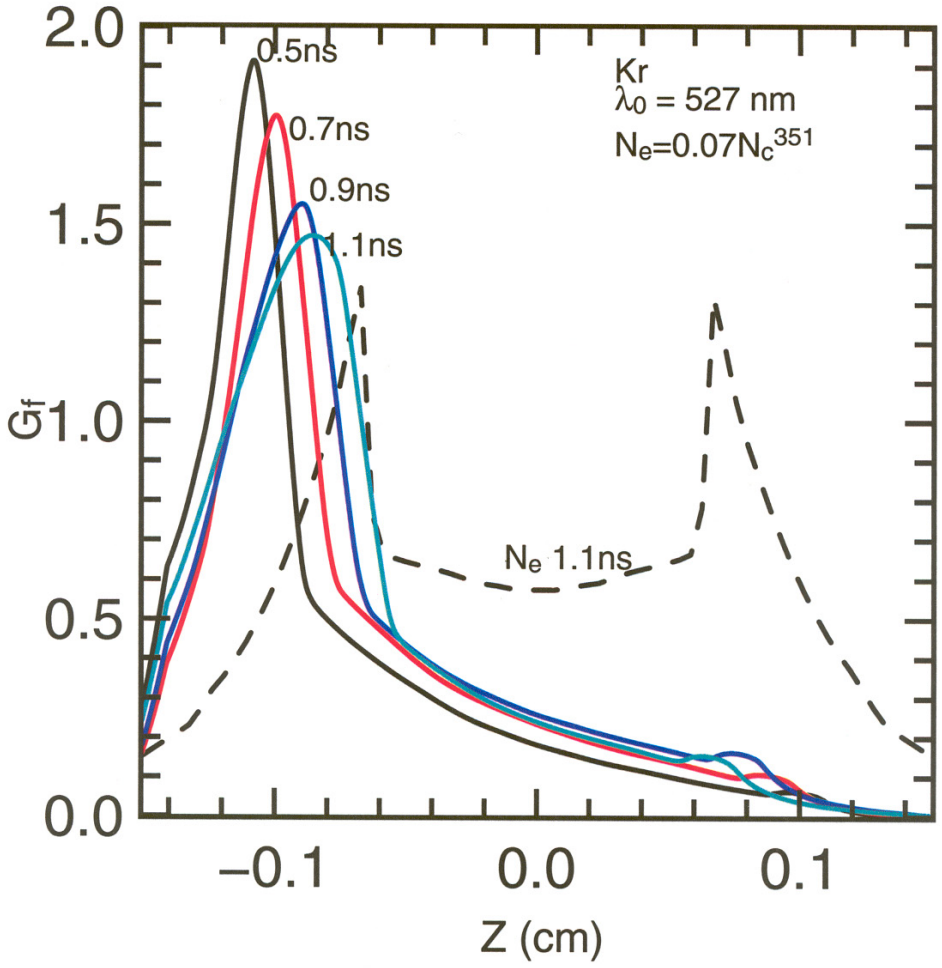

FIG. 9: The filamentation gain parameter G_f (see Eq. (12)) for 527nm light incident on a $0.07\mathrm{N_c^{351}}$ Krypton gasbag at 500ps (black line), 700ps (red line), 900ps (dark blue line), and 1100ps (light blue line). The electron density normalized to $1 \times 10^{21}\mathrm{cm}^{-3}$ at 1.1ns is also shown

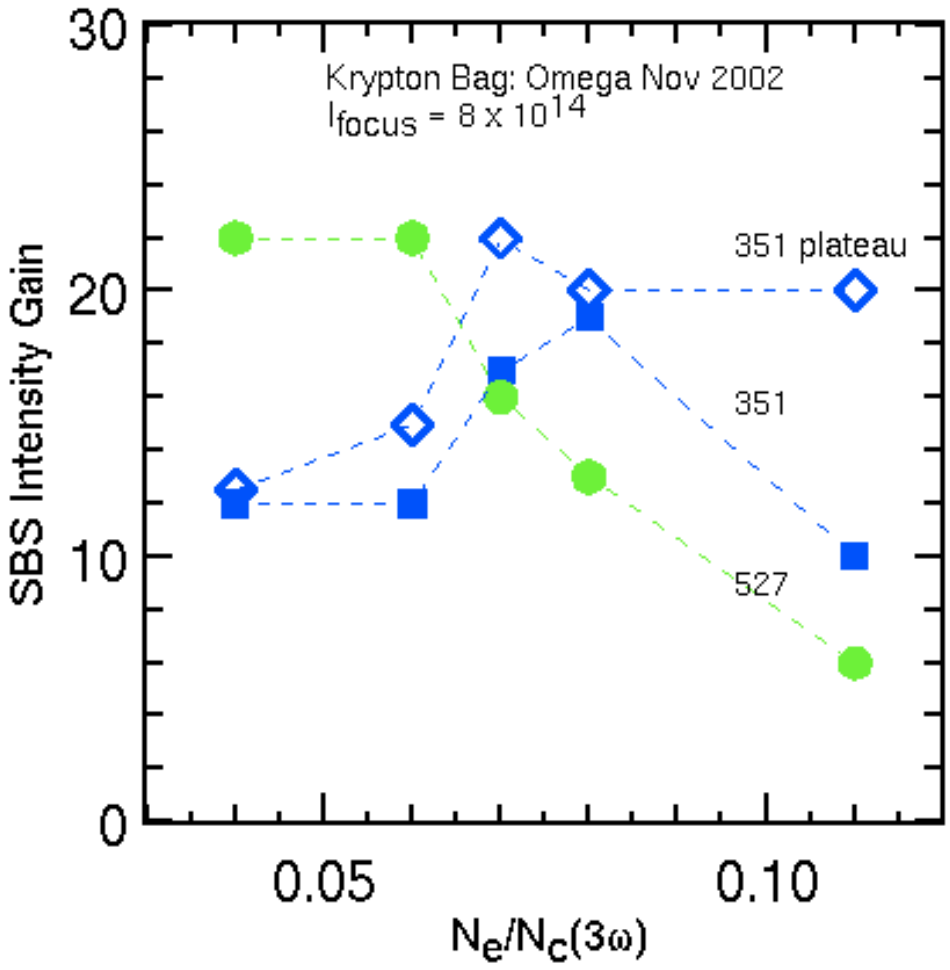

FIG. 10: The peak SBS gain for 527 nm (green circle) and 351 nm light (blue square) for constant incident power and focal spot size as a function of the Krypton gas electron density divided by the 351 nm critical density. The gain without the blast wave absorption or additional gain in the expanding plasma (open diamond) is also plotted. The peak gain for 351 nm light for a CO_2 fill with $N_e/N_c(351) = .04$ is about 30.

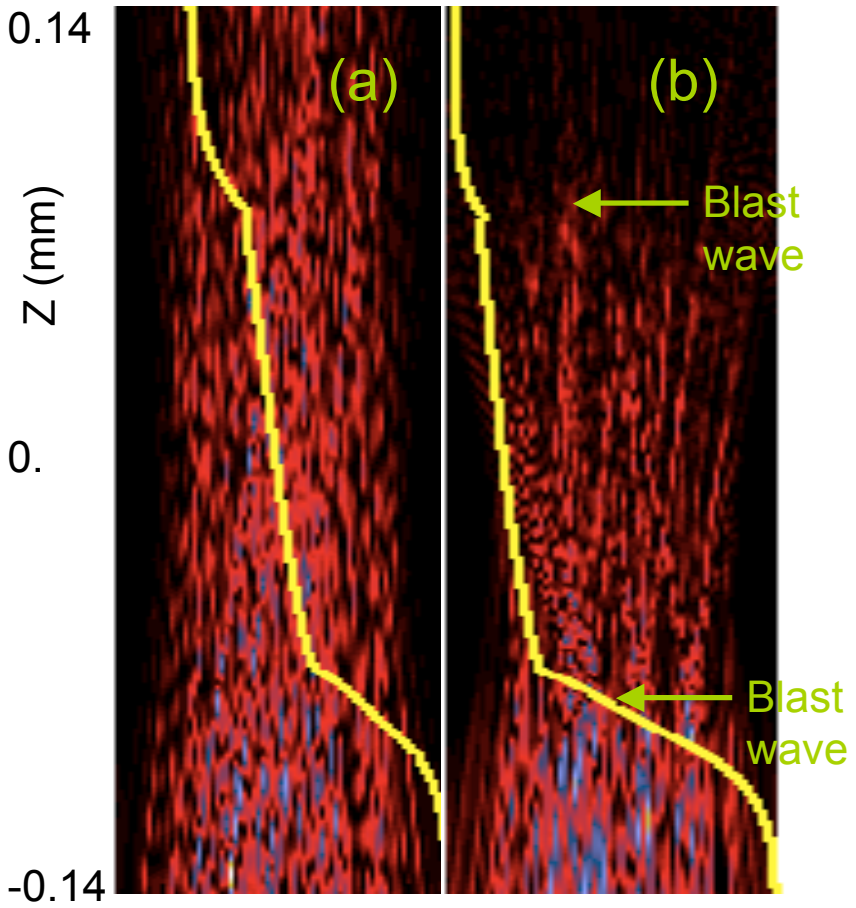

FIG. 11: A two dimensional slice of the simulated laser intensity propagated through a $0.07N_c^{351}$ Krypton-gas-filled bag for (a) 351nm and (b) 527 nm light. The overdrawn line is the laser power.

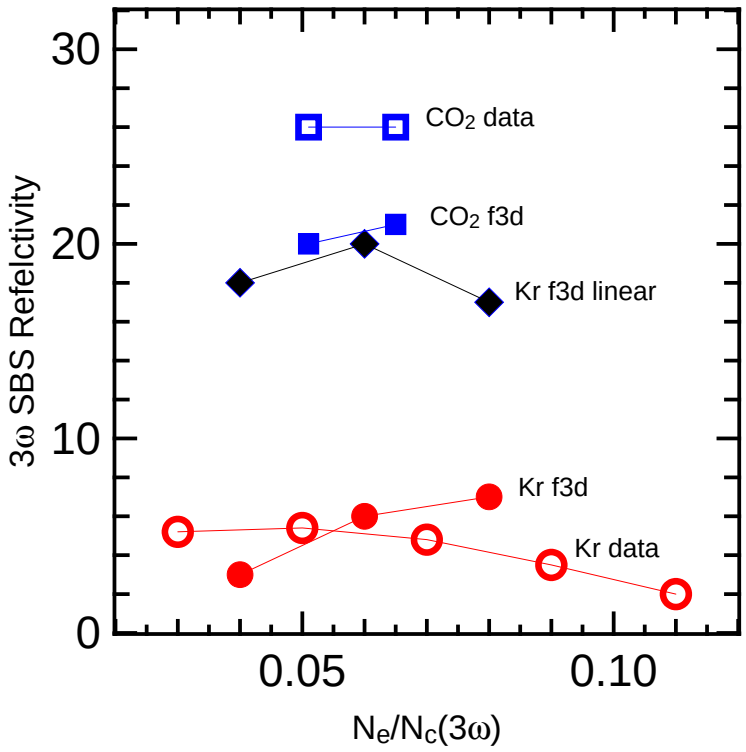

FIG. 12: The 351 nm light SBS reflectivity computed by pf3d simulations as a function of Krypton fill gas density and the measured reflectivity into the FABS detector at OMEGA. The simulation results are solid marks; the data are open marks.

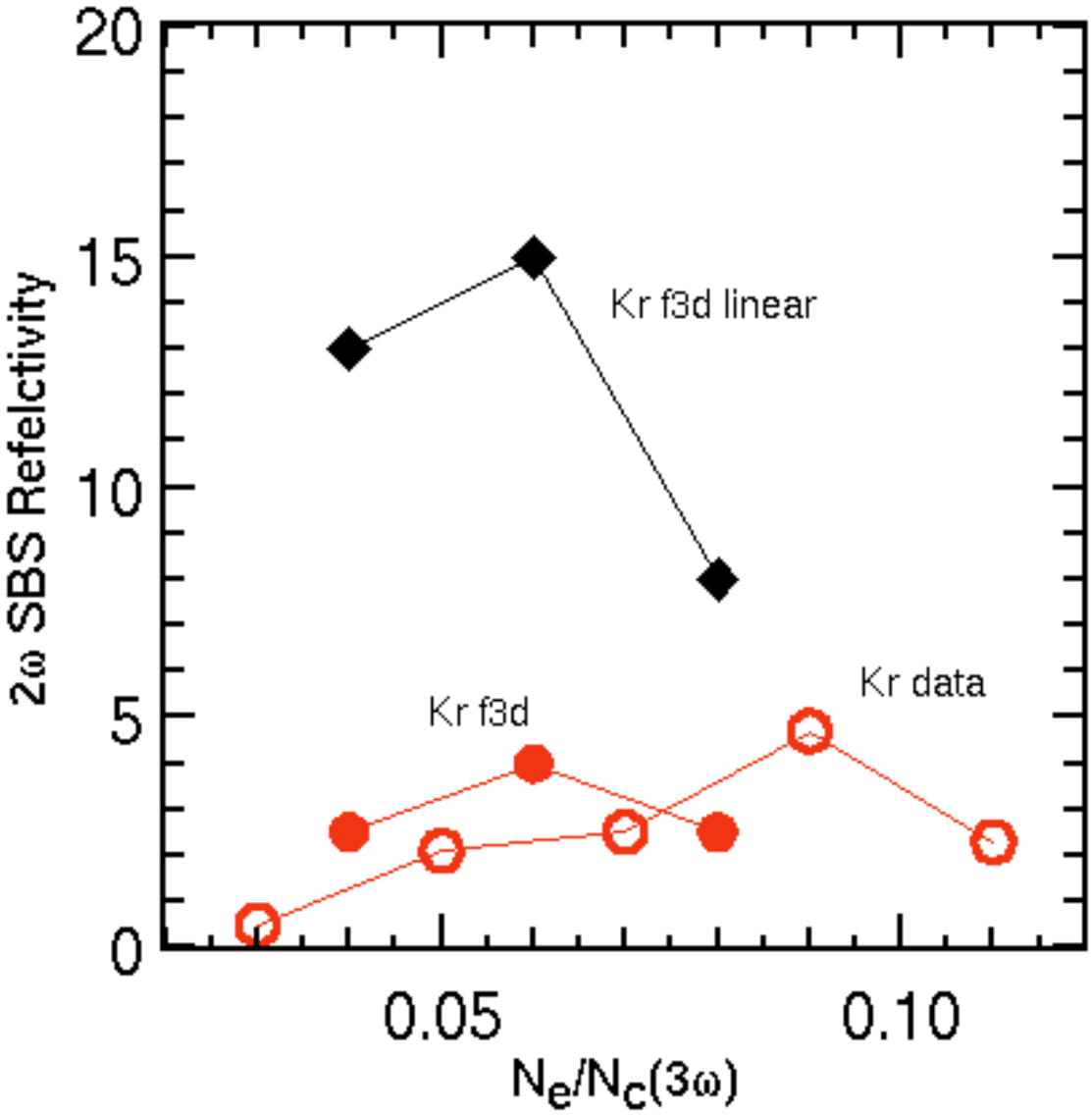

FIG. 13: The 527 nm light SBS reflectivity computed by pf3d simulations as a function of Krypton fill gas density and the measured reflectivity into the FABS detector at OMEGA. The simulation results are solid marks; the data are open marks.

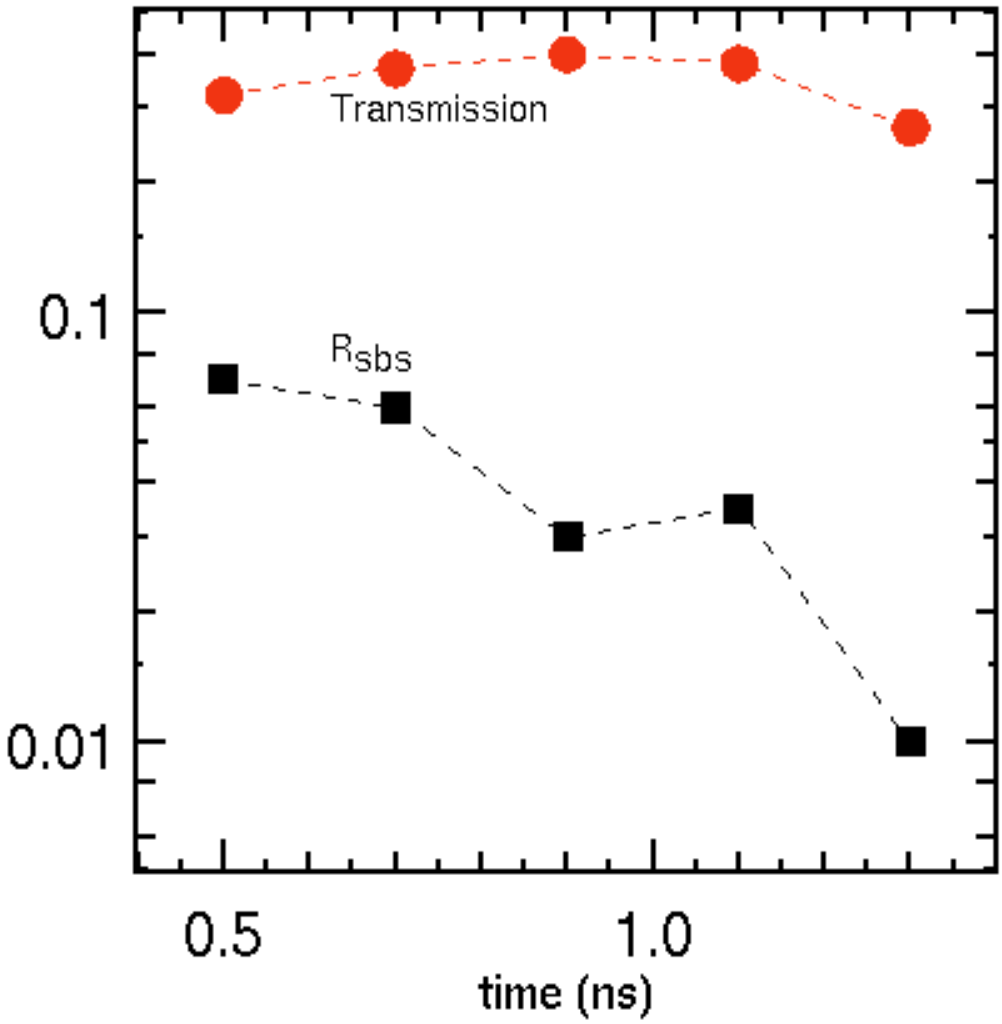

FIG. 14: The 351 nm SBS reflectivity and incident light transmission computed by pf3d simulations for the 4% Krypton fill density for the plasma conditions at 200 ps intervals. The simulations were 100-200 ps in duration.

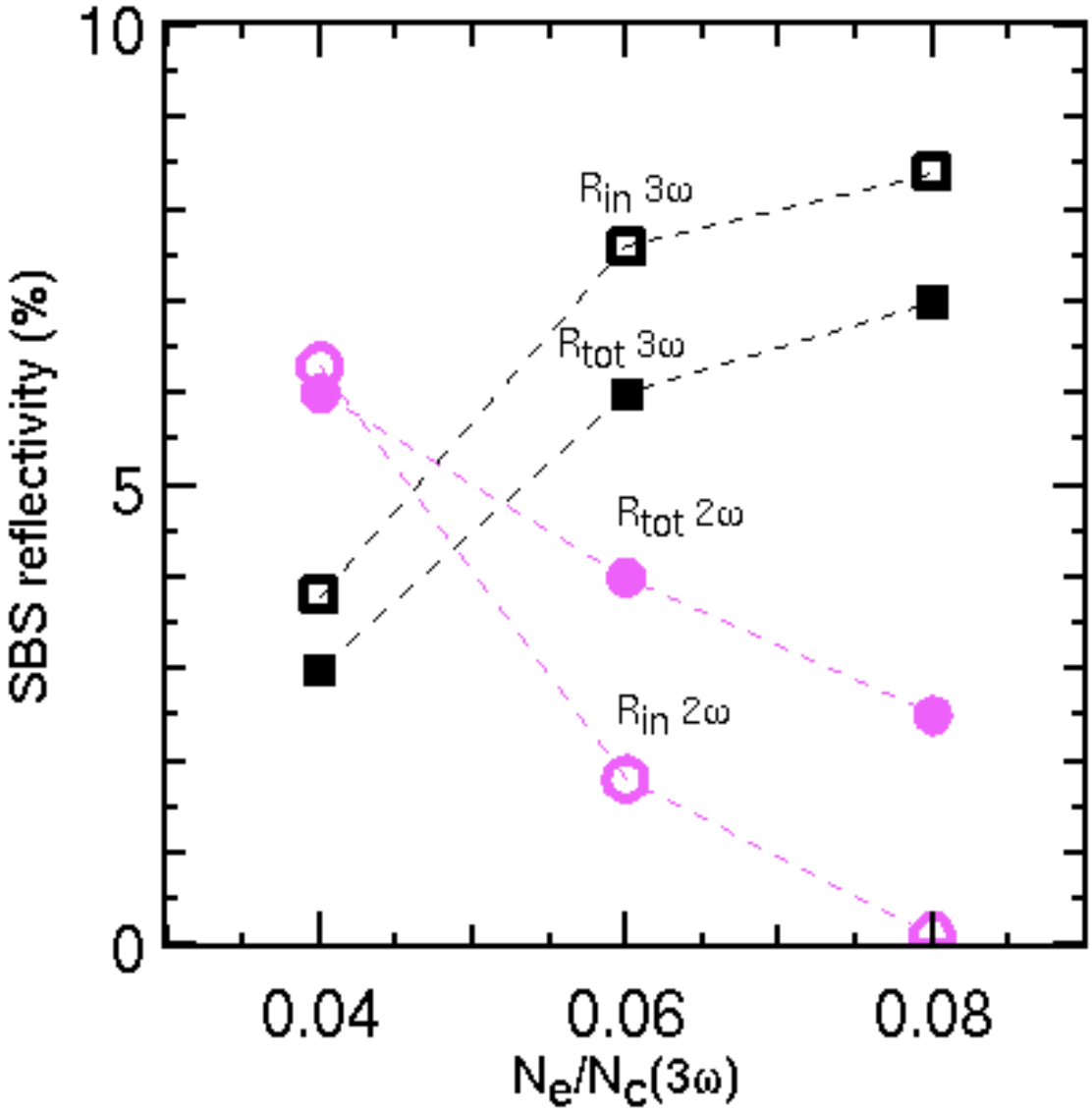

FIG. 15: The 351 nm and 527 nm SBS reflectivities computed by pf3d simulations versus Kr fill density for the plasma conditions at 900 ps. R_{in} is the reflectivity computed by dividing the reflected light energy before transmission through the blast wave by the laser light energy after transmission through the blast wave. R_{tot} is computed by dividing the reflected light energy after transmission through the blast wave by the incident light energy.

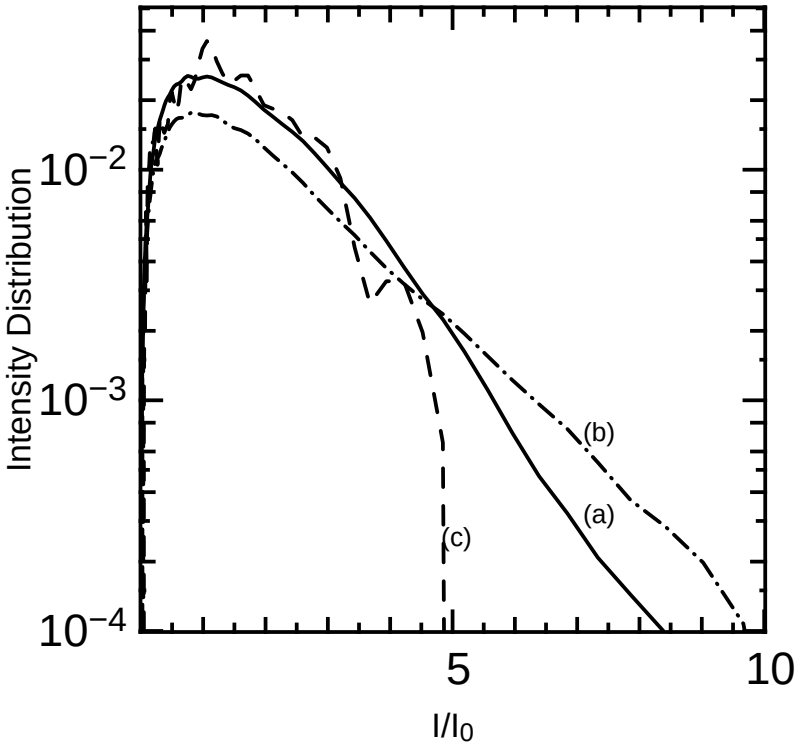

FIG. 16: The distribution of intensities for a 3D simulation of 527 nm light incident on a 7% Kr fill density for the plasma conditions at 900 ps (a) for the initial axial position and (b) for axial postion after focusing. Curve (c) is the initial distribution of intensities for a 2D simulation.